OXFORD

SOT | Society of Toxicology
www.toxsci.oxfordjournals.org

TOXICOLOGICAL SCIENCES, 2017, 1–13

doi: 10.1093/toxsci/kfx079
Advance Access Publication Date: April 29, 2017
Research article

Comparative Proteomics Reveals Silver Nanoparticles Alter Fatty Acid Metabolism and Amyloid Beta Clearance for Neuronal Apoptosis in a Triple Cell Coculture Model of the Blood–Brain Barrier

Ho-Chen Lin,[*,2] Ming-Yi Ho,[†,‡,2] Chao-Ming Tsen,[*,§] Chien-Chu Huang,[*] Chin-Ching Wu,[¶] Yuh-Jeen Huang,[*] I-Lun Hsiao,[*] and Chun-Yu Chuang[*,1]

[*]Department of Biomedical Engineering and Environmental Sciences, National Tsing Hua University, Hsinchu 30013, Taiwan; [†]Chromatography & Mass Spectrometry, Thermo Fisher Scientific, Taipei 11493, Taiwan; [‡]Institute of Stem Cell and Translational Cancer Research, Chang Gung Memorial Hospital, Taoyuan 33305, Taiwan; [§]Residue Control Division, Agricultural Chemicals and Toxic Substances Research Institute, Council of Agriculture Executive Yuan, Wufong, Taichung 41358, Taiwan; and [¶]Department of Public Health, China Medical University, Taichung 40402, Taiwan

[1]To whom correspondence should be addressed. Fax: (886) 3-5718649. E-mail: cychuang@mx.nthu.edu.tw.

[2]These authors contributed equally to this study.

ABSTRACT

Silver nanoparticles (AgNPs) enter the central nervous system through the blood–brain barrier (BBB). AgNP exposure can increase amyloid beta (Aβ) deposition in neuronal cells to potentially induce Alzheimer's disease (AD) progression. However, the mechanism through which AgNPs alter BBB permeability in endothelial cells and subsequently lead to AD progression remains unclear. This study investigated whether AgNPs disrupt the tight junction proteins of brain endothelial cells, and alter the proteomic metabolism of neuronal cells underlying AD progression in a triple cell coculture model constructed using mouse brain endothelial (bEnd.3) cells, mouse brain astrocytes (ALT), and mouse neuroblastoma neuro-2a (N2a) cells. The results showed that AgNPs accumulated in ALT and N2a cells because of the disruption of tight junction proteins, claudin-5 and ZO-1, in bEnd.3 cells. The proteomic profiling of N2a cells after AgNP exposure identified 298 differentially expressed proteins related to fatty acid metabolism. Particularly, AgNP-induced palmitic acid production was observed in N2a cells, which might promote Aβ generation. Moreover, AgNP exposure increased the protein expression of amyloid precursor protein (APP) and Aβ generation-related secretases, PSEN1, PSEN2, and β-site APP cleaving enzyme for APP cleavage in ALT and N2a cells, stimulated Aβ40 and Aβ42 secretion in the culture medium, and attenuated the gene expression of Aβ clearance-related receptors, P-gp and LRP-1, in bEnd.3 cells. Increased Aβ might further aggregate on the neuronal cell surface to enhance the secretion of inflammatory cytokines, MCP-1 and IL-6, thus inducing apoptosis in N2a cells. This study suggested that AgNP exposure might cause Aβ deposition and inflammation for subsequent neuronal cell apoptosis to potentially induce AD progression.

Key words: silver nanoparticles; proteomic profiling; blood–brain barrier; tight junction protein; amyloid beta clearance; Alzheimer's disease.

Silver nanoparticles (AgNPs) have antibacterial properties and are widely used in consumer products, including wound dressings, textiles, toothpastes, food containers, and cosmetics. AgNPs can dissociate into Ag particles and Ag ions in suspension solutions (Speranza *et al.*, 2013), and both of them exert cytotoxic effects on cells (Chen *et al.*, 2016; Foldbjerg *et al.*, 2009). Oral administration of AgNPs (60 nm) in rats resulted in the dose-dependent accumulation of Ag in many tissues, including the blood, liver, lungs, kidneys, stomach, testes, and brain (Ji *et al.*, 2007). Oberdorster *et al.* (2004) indicated that AgNPs can translocate from the olfactory mucosa of the respiratory tract to the central nervous system (CNS) through the olfactory nerve. In a mouse model, AgNP exposure (50 nm) induces blood–brain barrier (BBB) destruction and astrocyte swelling, and causes neuronal degeneration (Tang *et al.*, 2009). In an *in vitro* BBB model constructed using primary rat brain microvessel endothelial cells, AgNPs (25 nm) induce the secretion of proinflammatory cytokines, interleukin (IL)-1β, IL-2, and tumor necrosis factor alpha, and increase BBB permeability (Trickler *et al.*, 2010). In neuronal cells, AgNPs (20 nm) induce the degradation of cytoskeleton components, perturbations of postsynaptic proteins, and mitochondrial dysfunction to stimulate cell apoptosis (Xu *et al.*, 2013).

Alzheimer's disease (AD) is a progressive neurodegenerative disorder. Amyloid beta (Aβ) 40/42-induced extracellular amyloid plaques and tau protein-induced intraneuronal neurofibrillary tangles are the two major pathological mechanisms of AD (Bloom, 2014). Aβ40/42 is generated from Aβ precursor protein (APP) through β- and γ-secretase-mediated enzymatic digestion (Sinha and Lieberburg, 1999). β-Secretase is also referred to as β-site APP cleaving enzyme (BACE), which is responsible for initiating Aβ generation. Enhanced β-secretase activity increases Aβ deposition in the brain of patients with AD (Hampel and Shen, 2009). Presenilin (PSEN) is a multiple-pass transmembrane protein that forms the catalytic core of γ-secretase (Smolarkiewicz *et al.*, 2013). Citron *et al.* (1997) demonstrated increased Aβ42 levels in the brain of PSEN1/PSEN2 transgenic mice. Aβ can be eliminated from the brain by p-glycoprotein (P-gp), an adenosine triphosphate (ATP)-binding cassette transporter, and low-density lipoprotein (LDL) receptor-related protein-1 (LRP-1), a member of the LDL receptor family (Basak *et al.*, 2012; Deane *et al.*, 2009; Yamada *et al.*, 2008). Both P-gp and LRP-1 can transport Aβ from the brain to the bloodstream (Lam *et al.*, 2001; Shibata *et al.*, 2000). Moreover, decreased Aβ clearance activity increases Aβ accumulation in the brain of patients with AD (van Assema *et al.*, 2012).

The BBB allows the passage of nutrients and prevents the toxic substances through the CNS (Liu *et al.*, 2012). Zonula occludens-1 (ZO-1), occludin, and claudin-5 are the main components of the tight junctions that maintain BBB integrity in brain endothelial cells (Yang and Rosenberg, 2011). ZO-1 is an important link between tight junction proteins (claudin and occludin) and perijunctional actin (Musch *et al.*, 2006). Aberrant tight junctions are associated with neurological disorders, including AD, Parkinson disease, and multiple sclerosis (Bednarczyk and Lukasiuk, 2011).

Our previous study revealed that AgNP-exposed mouse neuroblastoma neuro-2a (N2a) cells have increased Aβ40/42 deposition, which potentially leads to the development of neurodegenerative disorders (Huang *et al.*, 2015). However, the mechanism through which AgNPs modulate proteomic metabolism to facilitate passage through the BBB and consequently cause neurodegenerative disorders remains unclear. Therefore, this study constructed a triple cell coculture model using mouse brain endothelial (bEnd.3) cells, mouse brain astrocytes (ALT), and mouse neuroblastoma N2a cells to simulate AgNP exposure in the brain. After AgNP exposure, *in vitro* BBB integrity was evaluated by examining transmembrane permeability and tight junction proteins in bEnd.3 cells and tracing the localization of AgNPs in ALT and N2a cells. To determine the potency of AgNP exposure in AD development, the mechanisms of aberrant Aβ generation, Aβ clearance, and apoptosis in N2a cells underlying AgNP-induced inflammation were investigated through proteomic profiling and gene expression studies.

MATERIALS AND METHODS

AgNP exposure in triple cell coculture model. The 3–5 nm uncoated AgNPs (Gold Nanotech Inc., Taipei, Taiwan) used in this study were maintained in deionized (DI) water. The AgNPs remained in a uniform spherical shape in DI water. Based on the measurements recorded by a JEM2100 transmission electron microscope (JEOL, Tokyo, Japan), the average size of the AgNPs was 4.5 nm. The size of the AgNPs as measured according to dynamic laser scattering and their zeta potential in Dulbecco's modified Eagle medium (DMEM; Corning Inc., Corning, NY) supplemented with 10% fetal bovine serum (FBS, Invitrogen, Carlsbad, Canada) and DI water were 105.6 ± 20.26 and 114.5 ± 2.75 nm and -5.5 ± 1.67 and 6.28 ± 0.338 mV, respectively. The Ag ion concentration in the AgNP stock solution was measured as 0.17 μg/ml using a perfectION comb Ag/S2 combination electrode (Mettler-Toledo Inc., Columbus, OH).

ALT and bEnd.3 cells were cultured in DMEM (Corning Inc.) supplemented with 10% FBS (Invitrogen), 1% penicillin and streptomycin (Biowest, Loire Valley, France), and 1% L-glutamine (Invitrogen) in a cell incubator at 5% CO_2 and 37 °C. N2a cells were cultured in a medium identical to that for ALT cells, and 1% sodium pyruvate (Invitrogen) was added. A modified version of the construction procedure for the triple cell coculture model by Li *et al.* (2010) was used. The bottom side of transwell filters (pore size, 0.4 μm; Corning Inc.) was coated with collagen type I (8 μg/cm^2 in 0.02 N acetic acid; Corning Inc.) for 1 h. The filters were washed with phosphate-buffered saline (PBS; Genestar Biotech, Shanghai, China). ALT cells (2.44×10^4 cells/cm^2) were seeded on the bottom side of the transwell filters for 2 h. After incubation, bEnd.3 cells (10^5 cells/cm^2) were seeded on the top side of the transwell filters and incubated for 3 days. In addition, N2a cells (2.1×10^4 cells/cm^2) were seeded on a new six-well plate for 16 h. After incubation, the medium was replaced with a differentiation medium (DMEM/10% FBS containing 200 μM isobutylmethylxanthine and 30 μM forskolin) for 48 h. Finally, the transwell filters were combined with the six-well plate containing differentiated N2a cells to construct a triple cell coculture model (Figure 1). After model assembly, the bottom medium was replaced with 2 ml of DMEM/1% FBS. Subsequently, 2 ml of AgNPs at final concentrations of 1, 2, 3, and 4 μg/ml in the DMEM/1% FBS medium was added to the upper chamber of the transwell filters for 24 h incubation.

Detection of transendothelial electrical resistance and tight junction proteins and Evans blue determination. Transendothelial electrical resistance (TEER) values were measured using Millicell ERS-2 (Millipore, Bedford, MA) according to the manufacturer's instructions. In brief, after 24 h AgNP exposure, the medium in the upper and bottom chambers were replaced with fresh DMEM/10% FBS. Subsequently, the electrode was placed in the

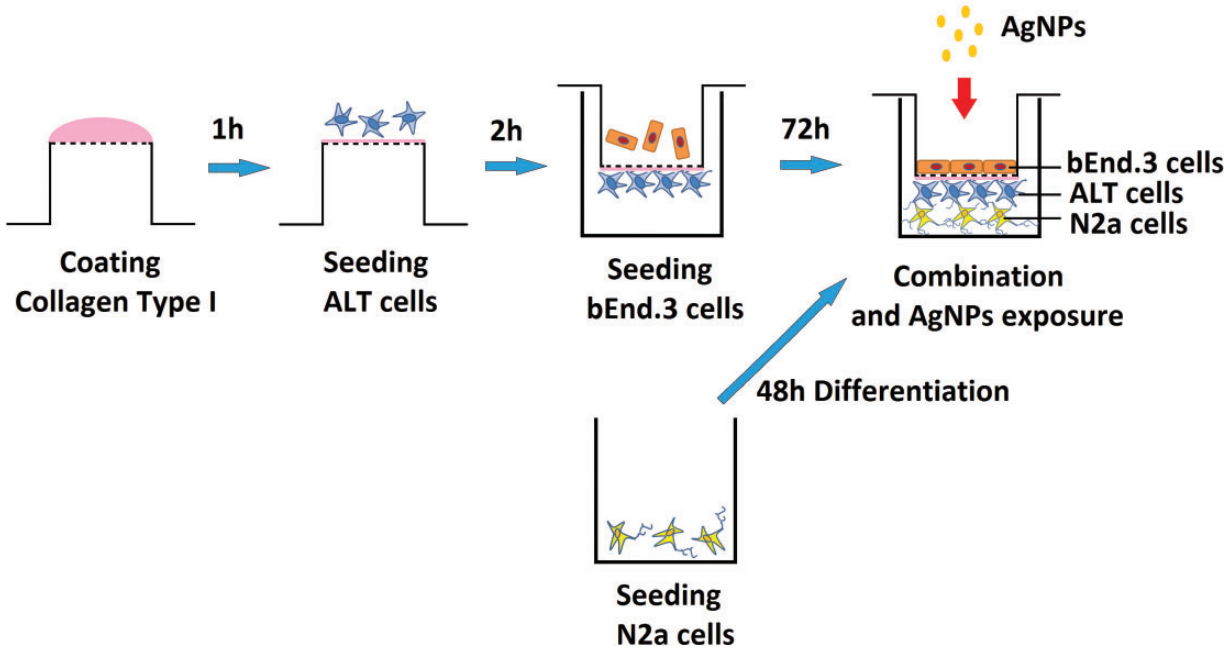

Figure 1. Construction of a triple cell coculture model.

upper and bottom chambers to measure TEER ($\Omega \times cm^2$) values. Results were corrected with blanks (DMEM/10% FBS).

$$\text{TEER } (\Omega \times cm^2) = [\text{TEER}_{sample}(\Omega) - \text{TEER}_{blank}(\Omega)] \times \text{area of membrane } (cm^2).$$

After exposing the triple cell coculture model to AgNPs, ALT cells on the bottom side of the transwell filter were removed using cotton swabs. The filter membrane with bEnd.3 cells was removed from the chamber, fixed with 4% paraformaldehyde (PFA), permeabilized with 0.1% Triton X-100/PBS solution, blocked in 2% horse serum, incubated with the rabbit anti-mouse ZO-1 (cat. 617300; Invitrogen) or claudin-5 primary antibody (cat. 341600; Invitrogen) for 1 h and the fluorescein isothiocyanate (FITC)-conjugated goat anti-rabbit immunoglobulin (IgG) secondary antibody for 1 h (cat. 12-507; Merck Millipore), and finally transferred to a coverslip and mounted in the mounting medium (Invitrogen). Immunofluorescence images were captured using an inverted microscope with fluorescence filters (Axio Observer A1/D1, Zeiss, Oberkochen, Germany).

In Evans blue determination, the upper and bottom chambers were washed with Hank's balanced salt solution (HBSS) after exposing the triple cell coculture model to AgNPs for 24 h. HBSS (1.5 ml) was added to the bottom chamber, and 0.5 ml of Evans blue staining solution (0.25% Evans blue [Chem-Impex, Wood Dale, IL, USA] and 4% bovine serum albumin in HBSS) was added to the upper chamber and incubated at 37°C for 5 min. The solution in the bottom chamber was collected, and absorbance at 610 nm was measured using a UV/vis spectrometer (Optizen POP BIO, Mecasys, Korea).

Reverse transcription and quantitative real-time polymerase chain reaction. Total RNA was extracted from bEnd.3, ALT, and N2a cells in the triple cell coculture model after 24 h AgNP exposure by using RNA Trizol (Invitrogen). The quantity and purity of RNA samples were assessed using NanoDrop 2000c (Thermo Fisher Scientific, Wilmington, DE). The absorbance ratios of acceptable RNA purity were established as A260/A280 $\geq$ 1.8 and A260/A230 $\geq$ 1.5.

Complementary DNA (cDNA) was synthesized from 3 μg of total RNA by using a high-capacity cDNA reverse transcription kit (Applied Biosystems, Foster City, CA). A real-time polymerase chain reaction (PCR) was performed to amplify 100 ng of cDNA in 40 cycles using the 2× power SYBR green PCR master mix (Applied Biosystems). The primer sequences used in this study were as follows: β-actin sense 5′-ATG CTC CCC GGG CTG TAT-3′ and antisense 5′-GCT CTG GGC CTC GTC ACC-3′; BACE sense 5′-CAA AAC TGG GAA AGG CAG AAC TC-3′ and antisense 5′-CAG ACT ACA ACC ACA GGC ACA TT-3′; claudin-5 sense 5′-TGG ATG TCG TGC GTG GTG-3′ and antisense 5′-GGT CAA GGT AAC AAA GAG TGC C-3′; LRP-1 sense 5′-CAG CCA GAA GTG TGA CCA GAA C-3′ and antisense 5′-TCC AAG ACC CAG CCC TCG TA-3′; P-gp sense 5′-TCA TCG CTT GTC TAC CGT TCG T-3′ and antisense 5′-TTT CAT TTC CTG CTG TCT GTG TCA T-3′; PSEN1 sense 5′-AGC AAC CGC CAG TGG AGA C-3′ and antisense 5′-CGA AGT AGA ACA CGA GCC C-3′; PSEN2 sense 5′-GCC TGG GTC ATC TTG GGT G-3′ and antisense 5′-TTT CTC TCC TGG GCA GTT TCC-3′; and ZO-1 sense 5′-ACC CGA AAC TGA TGC TGT GG-3′ and antisense 5′-GCC CTT GGA ATG TAT GTG GAG AGA A-3′. Quantitative analysis of PCR products was conducted using a sequence detector (Model 7300, Applied Biosystems), according to the manufacturer's instructions. The signal of SYBR green was measured at 530 nm during the extension phase and detected and analyzed using SDS 1.0 software (Applied Biosystems). The relative level of mRNA expression was defined as a ratio of the optical density of the experimental groups to that of an endogenous house-keeping gene β-actin.

Determination of total Ag concentration and AgNP localization in neuronal cells. One milliliter of the medium or harvested ALT and N2a cells was pretreated with 0.5 ml of pure nitrate (Sigma-Aldrich, St. Louis, MO) and digested at 75 °C for 16 h. DI water was added to the treated samples to attain a volume of 5 ml. The total Ag concentration in these samples was measured using an inductively coupled plasma mass spectrometer (ELAN

DRC II, PerkinElmer, Norwalk, CT). $AgNO_3$ was used as a standard with concentrations ranging from 0.5 to 1000 μg/l to plot a standard curve.

In the AgNP localization experiment, N2a cells were cultured and differentiated on glass coverslips before constructing the triple cell coculture model. After the triple cell coculture model was exposed to AgNPs (4 μg/ml) for 24 h, bEnd.3 cells in the upper chamber were removed using cotton swabs, and the membrane was cut off from the chamber. The membrane with ALT cells and glass coverslips with N2a cells were rinsed with a mixture of tripotassium hexacyanoferrate (III) (10 mM; Sigma-Aldrich) and sodium thiosulfate pentahydrate (10 mM; Sigma-Aldrich) to remove AgNPs from the cell surface. The cells were fixed in 4% PFA and covered with ProLong antifade mountant and 4′-6-diamidino-2-phenylindole (DAPI; Life Technologies Inc., Carlsbad, CA) for nuclear staining. Images were captured using a confocal laser scanning microscope (LSM 780; Carl Zeiss, Göttingen, Germany) with a ×63 oil-immersion objective; a 561-nm laser was used for imaging AgNPs in the reflectance mode, and a 405-nm laser was used for DAPI.

Protein extraction for quantitative proteomic analysis and fatty acid determination. N2a cells (25 μl cell pellet from the six-well plate) were lysed by mixing them with 150 μl of lysis buffer containing 5% sodium deoxycholate, 10 mM dithiothreitol, and 0.1 M triethylammonium bicarbonate with 1% protease inhibitor cocktail and incubated at 95 °C for 10 min. Before enzymatic digestion with sequencing grade trypsin (cat. V5111, Promega, Madison, WI), the lysate was clarified through sonication and centrifugation at 14 000 × g for 10 min, and the protein content was determined through the Bradford protein assay. An aliquot of lysate containing 400 μg of proteins was transferred to the top of 30-kDa centrifugal filter units (Millipore, Microcon) and digested according to the filter-aided sample preparation methods described by Wisniewski *et al.* (2009) and Leon *et al.* (2013). After overnight digestion, peptide samples were recovered through acidification (final 0.5% trifluoroacetic acid), followed by phase transfer with ethyl acetate extraction (Masuda *et al.*, 2008). The peptide solution was dried using SpeedVac (Thermo Fisher Scientific) and desalted using a Sep-Pak C18 SPE cartridge (Waters Inc., Milford, MA). The concentration of the peptide solution was determined using NanoDrop (1 mg/ml solution has 1.1 au at 280 nm). Furthermore, 100 μg of each peptide sample was aliquoted and labeled with tandem mass tags (TMTs; Thermo Fisher Scientific), according to the manufacturer's instructions. Proteomic analysis was conducted through nanoscale liquid chromatography–tandem mass spectrometry using an Orbitrap Fusion Tribrid mass spectrometer (Thermo Fisher Scientific) according to Tan *et al.* (2016). Quantitative proteomic analysis was performed using Proteome Discoverer v2.1 software.

Differentially expressed proteins (DEPs) were screened based on false discovery rate (FDR) confidence (high and medium) and fold changes of TMT intensity (>1.2 or <0.833) in the AgNP (4 μg/ml) exposure group and control group. The DEPs were functionally classified through gene ontology analysis using the DAVID website (http://david.abcc.ncifcrf.gov/; last accessed May 4, 2017). The Cytoscape (version 3.02) ClueGO + CluePedia plug-in system was used to identify the gene networks and functional pathways of DEPs. A two-sided hypergeometric statistic was calculated with a kappa score threshold setting of 0.4.

For fatty acid determination, ALT and N2a cells were harvested with trypsin (Invitrogen) and washed with PBS. Methanol was added to the cells, and sonication was performed for 10 min at room temperature. The supernatant was transferred to a new tube and dried using nitrogen at room temperature. Samples were dissolved in 200 μl of acetonitrile, and 50 μl of n-tert-butyldimethylsilyl-n-methyltrifluoroacetamide (Sigma-Aldrich) was added. These samples were incubated at 70 °C for 40 min. Samples were analyzed using Agilent GC 7890A coupled with a single quadrupole MSD 5975C (Agilent Technologies, Palo Alto, CA) system, and separated using a HP-5MS column (60 m × 0.25 mm × 0.25 μm; Agilent Technologies). After 1 μl of sample was injected, the GC oven was maintained at 60 °C for 1 min. Subsequently, the temperature of the GC oven was increased to 325 °C at 10 °C/min, followed by a 5-min hold at 325 °C. The injection port temperature was maintained at 250 °C throughout the determination. The data were analyzed using MSD ChemStation (Agilent Technologies, version G1701EA E.01.00.237).

Western blotting. N2a and ALT cells were lysed with the radioimmunoprecipitation assay buffer (Cell Signaling, Danvers, MA) containing a protease inhibitor cocktail (Sigma-Aldrich) and centrifuged at 14 000 × g for 10 min at 4 °C. The total protein concentration in samples was determined using a bicinchoninic acid protein assay kit (Sigma-Aldrich). The protein samples were electrophoresed on a 10% sodium dodecyl sulfate–polyacrylamide gel and subsequently transferred to a hydrophobic polyvinylidene fluoride membrane (Millipore). The membrane-bound proteins were immunostained with 1:1000 rabbit anti-mouse APP (cat. EPR 5118-34; Abcam, Cambridge, UK), BACE (cat. GTX103757; GeneTex, Irvine, CA), PSEN1 (cat. GTX116016; GeneTex), PSEN2 (cat. GTX55758; GeneTex), or β-actin primary antibody (cat. sc-4778; Santa Cruz Biotechnology, Santa Cruz, CA), followed by treatment with the anti-rabbit IgG horseradish peroxidase secondary antibody (cat. sc-2301; Santa Cruz Biotechnology). The tagged proteins were detected using a chemiluminescence reagent (Thermo Fisher Scientific) and photographed in a G:Box ChemiXT16 system (Syngene, Frederick, MD). The densitometric analysis of Western blot results was conducted using Image J software.

Quantification of Aβ40, Aβ42, and inflammatory cytokines. The Aβ40 concentration of the medium in the upper and bottom chambers was determined using a commercially available enzyme-linked immunosorbent assay (ELISA) kit (AnaSpec, Fremont, CA). First, 50 μl of a dilute detection antibody and 100 μl of the medium were added to a 96-well plate, and the plate was incubated at 4 °C for 16 h. After incubation, the wells were washed seven times with 1× wash buffer, and 100 μl of tetra methyl benzidine (TMB) color substrate solution was added to each well and incubated at room temperature for 20 min. Finally, 50 μl of stop solution was added to each well. The absorbance values were measured at 450 nm using a microplate reader (Molecular Devices, Sunnyvale, CA). The Aβ42 concentration was determined using an Aβ42 ELISA kit (cat. EM0864; FineTest, Wuhan, China). Two hundred microliters of the medium was added to an Aβ42 antibody-coated 96-well plate and incubated at 37 °C for 90 min. The plate content was discarded, 100 μl of a biotin detection antibody was added, and the plate was incubated at 37 °C for 60 min. The plate was washed three times with wash buffer, 100 μl of SABC solution was added, and the plate was incubated at 37 °C for 30 min. The plate was washed five times with wash buffer, 90 μl of TMB substrate was added, and the plate was incubated at 37 °C in the dark for 15 min. Finally, 50 μl of stop solution was added to the plate, and the absorbance values were measured at 450 nm using the microplate reader (Molecular Devices). The concentration of inflammatory

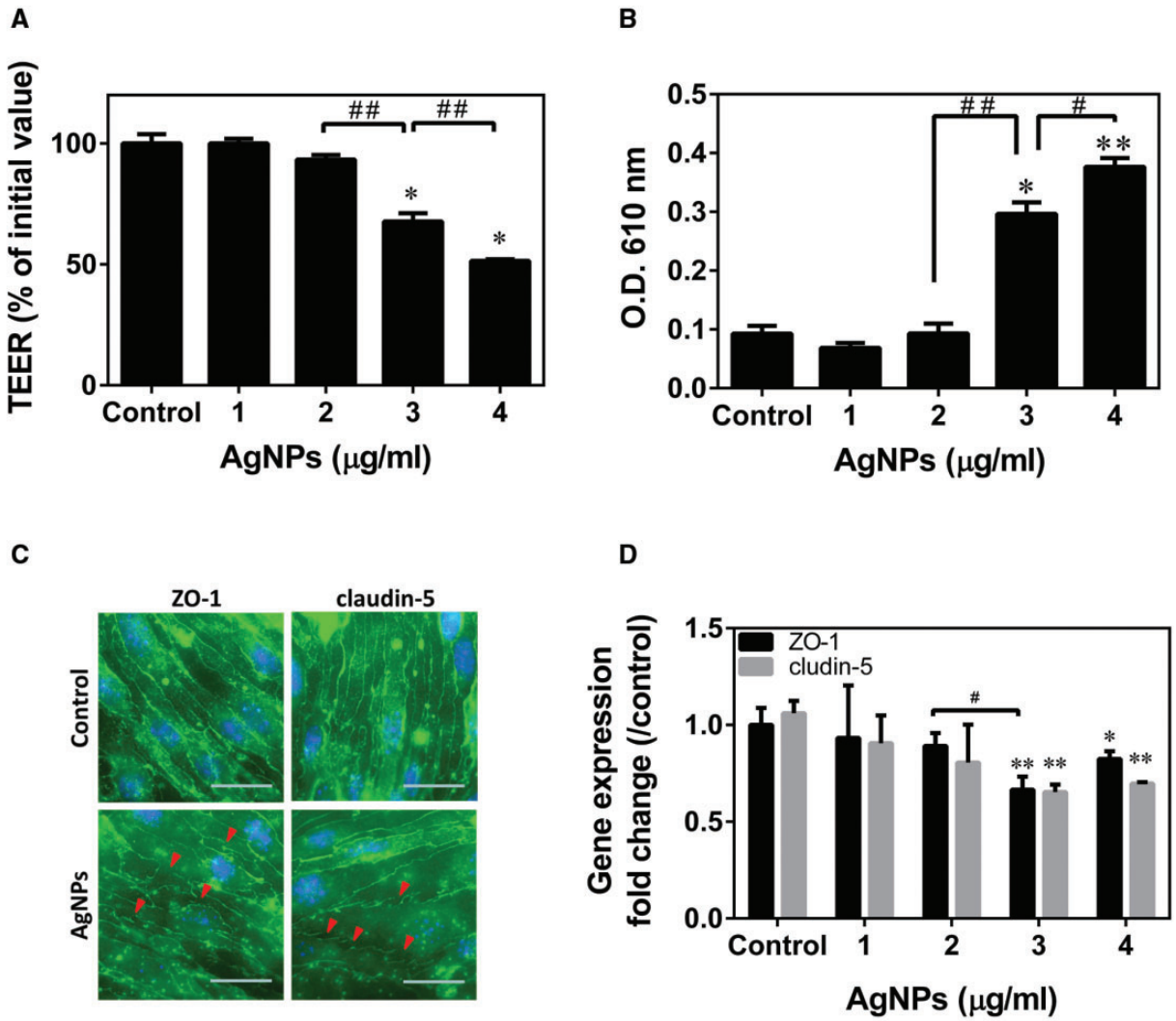

Figure 2. Transendothelial electrical resistances, Evans blue determination, and gene expression of tight junction proteins in a triple cell coculture model after AgNP exposure. A, The triple cell coculture model was treated with various concentrations of AgNPs (1, 2, 3, and 4 μg/ml) for 24 h. The determined TEER values are expressed in $\Omega \times cm^2$ as the mean ± standard deviation (SD). Results were presented in percentages compared with the control group ($n = 6$). B, *In vitro* BBB permeability was evaluated based on Evans blue absorbance at 610 nm in the bottom medium. Results were presented as the mean ± SD ($n = 6$). After the triple cell coculture model was treated with AgNPs for 24 h, the gene and protein expression levels of claudin-5 and ZO-1 in bEnd.3 cells were individually measured using (C) an immunofluorescence microscope with ×600 magnification; blue, nucleus; green, tight junction proteins; red arrow, AgNPs disrupt the integrity of tight junction proteins on the cell surface. Scale bar = 25 μm. D, Real-time PCR (fold changes of AgNP exposure compared with the control group) were presented as the mean ± SD ($n = 6$). These reactions were performed in duplicate in three independent experiments. $^{*}P < .05$; $^{**}P < .01$, significantly different from the control group; $^{\#}P < .05$ and $^{\#\#}P < .01$, significantly different between the two exposure groups.

cytokines in the medium in the upper and bottom chambers were measured using a Bio-PlexMouse Cytokine 23-Plex panel (Bio-Rad Laboratories Inc., Hercules, CA).

Cell apoptosis assay. Cell apoptosis was observed using an Annexin-V detection kit (Invitrogen) in N2a cells after the triple cell coculture model was exposed to AgNPs. One million cells were washed with PBS and resuspended in binding buffer (10 mM 4-(2-hydroxyethyl)-1-piperazineethanesulfonic acid/NaOH, pH 7.4; 140 mM NaCl; 2.5 mM $CaCl_2$). Annexin V-FITC (100 ng/ml) was added to the cell solution and incubated in the dark for 10 min, washed with PBS, and resuspended in 500 μl of binding buffer. Prior to flow cytometric analysis, 10 μl of propidium iodide (1 mg/ml; Invitrogen) was added to each sample. The cells were analyzed using a FACSCanto flow cytometer (BD Biosciences, San Jose, CA). In each sample, 10 000 cells were counted. Data analysis was performed using WinMDI software (version 2.9; Scripps Research Institute, San Diego, CA).

Statistical analysis. Statistically significant differences in the gene expression, protein expression, Evans blue concentration, cytokine concentration, and total Ag concentration of the AgNP exposure and control groups were analyzed through one-way analysis of variance (GraphPad 6.0). A two-tailed P value $< .05$ was considered to indicate statistical significance.

RESULTS

Tight Junctions in bEnd.3 Cells After AgNP Exposure

After the triple cell coculture model was exposed to AgNPs (2, 3, and 4 μg/ml) for 24 h, the TEER values of bEnd.3 cells decreased

Table 1. Silver Concentration in the Bottom Medium, Astrocytes, and Neuronal Cells After a Triple Cell Coculture Model Exposure to AgNPs

Groups	Ag Concentration (μg/l)			% of Initial AgNPs Exposure		
	Bottom Medium	ALT Cells	N2a Cells	Bottom Medium	ALT Cells	N2a Cells
Control	N.D.	N.D.	N.D.	–	–	–
AgNPs (1 μg/ml)	8.67±0.53	1.85±0.09	6.17±0.31	0.87±0.05	0.19±0.01	0.62±0.03
AgNPs (2 μg/ml)	49.08±2.37*	3.87±0.08*	24.70±0.61*	2.45±0.12*	0.19±0.00	1.24±0.03*
AgNPs (4 μg/ml)	192.68±10.43*,#	19.83±2.72*,#	52.62±12.29*,#	4.82±0.26*,#	0.50±0.07*,#	1.32±0.31*

% of initial AgNPs exposure: % of detected Ag concentration/concentration of AgNPs exposure.
ND, not detectable.
*$P < .05$ compared with AgNPs 1 μg/ml.
#$P < 0.05$ compared with AgNPs 2 μg/ml.

in a dose-dependent manner (Figure 2A). Evans blue determination revealed that AgNPs at 3 and 4 μg/ml increased the permeability of the triple cell coculture model (Figure 2B). The integrity of tight junction proteins, ZO-1 and claudin-5, was disrupted after AgNP exposure at 4 μg/ml (Figure 2C). Furthermore, AgNP (3 and 4 μg/ml) exposure reduced the gene expression of ZO-1 and claudin-5 in bEnd.3 cells (Figure 2D).

AgNP Distribution in Astrocytes and Neuronal Cells

After exposure of the triple cell coculture model to AgNPs (1, 2, and 4 μg/ml), the total Ag was detected to move from the medium to ALT and N2a cells (Table 1). After exposure to AgNPs at 4 μg/ml, the percentage of AgNP concentrations in the bottom medium, ALT cells, and N2a cells were 4.82 ± 0.26%, 0.51 ± 0.07%, and 1.31 ± 0.31%, respectively. Confocal microscopy imaging revealed that AgNPs were located in the cytoplasms of ALT and N2a cells after AgNP exposure at 4 μg/ml (Figure 3).

Proteomic Metabolism in N2a Cells After AgNP Exposure

Total protein in N2a cells was labeled with TMTs after the triple cell coculture model was exposed to AgNPs. In proteomic analysis, 298 DEPs (upregulated, $n = 38$; downregulated, $n = 268$) were identified from 5953 proteins (Figure 4A; Supplementary Table 1). Molecular function analysis (Supplementary Figure 1A) revealed that these proteins were involved in catalytic activity, binding, structural molecular activity, and receptor activity. In addition, biological function analysis (Supplementary Figure 1B) indicated that these DEPs were associated with metabolic process, cellular process, localization cellular component organization of biogenesis and biological regulation. Furthermore, Kyoto Encyclopedia of Genes and Genomes (KEGG) pathway analysis (Table 2) demonstrated that DEPs were involved in ribosome biogenesis, oxidative phosphorylation, insulin signaling pathways, fatty acid elongation, and neuronal diseases, such as Parkinson disease, Huntington disease, and AD. Cytoscape gene-network analysis revealed that DEPs were associated with ribosome biogenesis, protein localization to the endoplasmic reticulum, posttranslational protein modification, endoplasmic reticulum organization, mitochondrion organization, ribonucleoside metabolism, Parkinson's disease, and Huntington's disease (Figure 4B). Subnetwork analysis showed that AgNPs modulated fatty acid metabolism-related proteins, including insulin, peroxisome proliferator-activated receptor alpha (PPARα), protein kinase adenosine monophosphate (AMP)-activated catalytic subunit α2, malonyl-coA decarboxylase, protein kinase AMP-activated noncatalytic subunit gamma (PRKAG) 1, PRKAG2, and peroxisome proliferator-activated receptor gamma coactivator 1α (PPARGC1α), to activate cytochrome c, somatic (CYCS), and caspase 3 (CASP3) for cell apoptosis (Figure 4C).

Fatty Acid Composition in Neuronal Cells After AgNP Exposure

After exposure of the triple cell coculture model to AgNPs, the total fatty acid composition in ALT and N2a cells was determined through gas chromatography and mass selective detection. After AgNP exposure at 4 μg/ml, the palmitic acid concentration significantly increased (fold change, 1.35 ± 0.02) in N2a cells, and no apparent changes were observed in ALT cells (Table 3).

Aβ Determination After AgNP Exposure

After the triple cell coculture model was exposed to AgNPs, gene and protein expression results revealed that APP was induced in N2a cells in a dose-dependent manner (Figs. 5A and B). AgNPs at 2 μg/ml significantly increased the secretion of Aβ40 (113 ± 4%) and Aβ42 (107 ± 3%) into the bottom medium compared with the control group, and no apparent changes were observed in the upper medium (Figure 5C). Moreover, the gene expression of Aβ generation-related secretases, namely PSEN1, PSEN2, and BACE, in ALT and N2a cells (Figure 5D) was significantly increased after AgNP exposure. The protein expression of BACE in ALT cells and that of PSEN1 and PSEN2 in N2a cells was also increased after AgNP exposure (Figure 5E). The gene expression of Aβ clearance-related receptors, namely LRP-1 and P-gp, in bEnd.3 cells was significantly decreased after AgNP exposure at 2 and 4 μg/ml (Figure 5F).

Inflammatory Cytokine Secretion and Cell Apoptosis in Neuronal Cells After AgNP Exposure

In the triple cell coculture model, AgNP exposure at 4 μg/ml induced IL-6 and MCP-1 secretion and decreased IL-1β secretion in the upper medium containing bEnd.3 cells and MCP-1 secretion in the bottom medium containing ALT and N2a cells (Figs. 6A and B). AgNPs (4 μg/ml) induced early and late apoptosis in 10.8% and 26.2% of N2a cells, respectively (Figure 6C).

DISCUSSION

AgNPs have been used in consumer products for many years. However, their effects on neurodegenerative disorders remain unclear. Our previous studies have revealed that AgNPs can induce inflammation and enhance Aβ accumulation in monocultured N2a cells (Huang *et al.*, 2015; Lin *et al.*, 2016). The present study used molecular and proteomic approaches to investigate the adverse effects of AgNPs on neuronal cells. This study demonstrated that AgNPs can traverse through the

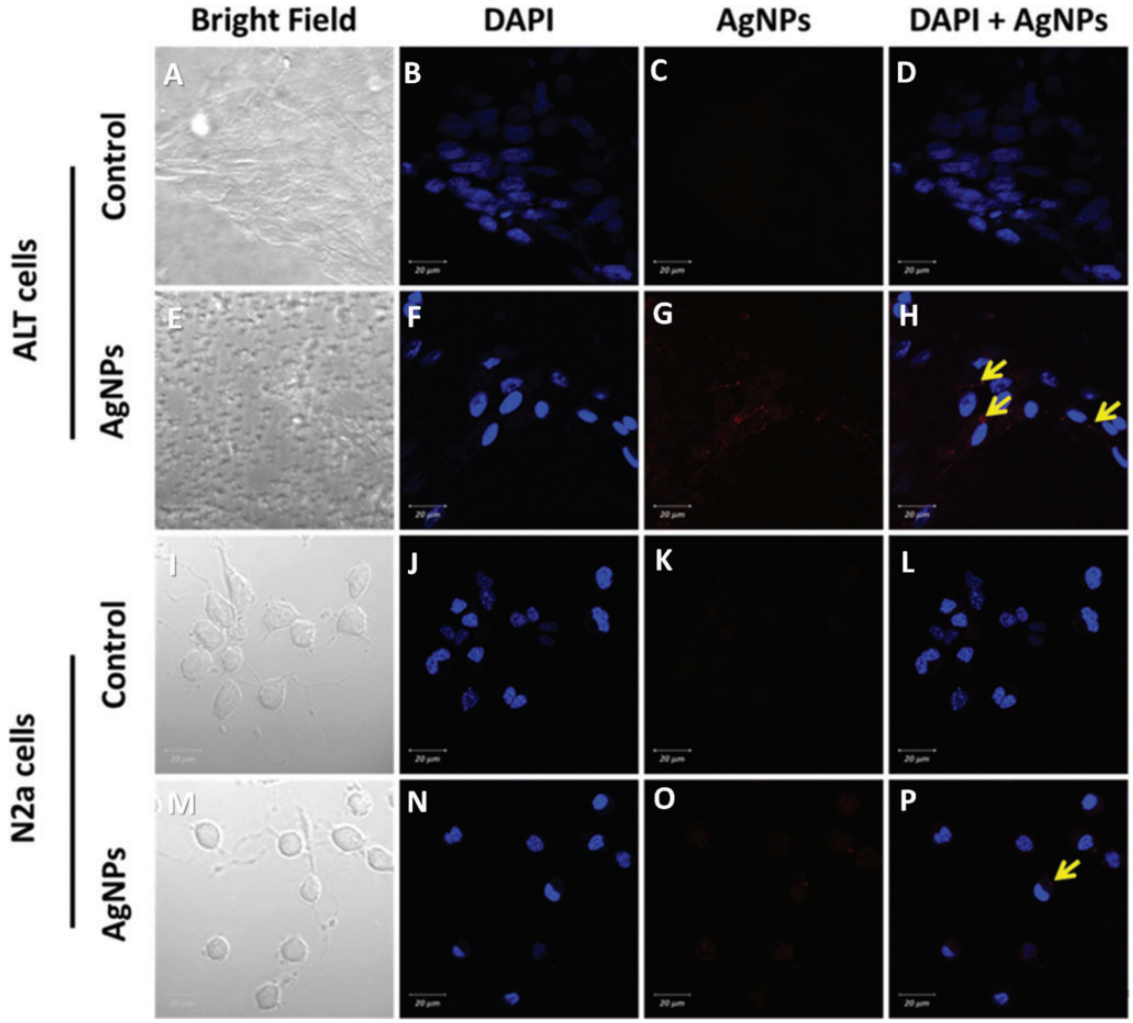

Figure 3. AgNP uptake in ALT and N2a cells of the triple cell coculture model. After the triple cell coculture model was exposed to AgNPs (4 μg/ml) for 24 h, AgNP uptake in ALT cells (A–H) and N2a cells (I–P) was examined through confocal microscopy. Bright field images (A, E, I, and M), images of DAPI (B, F, J, and N) and AgNPs (C, G, K, and O), and merged images (D, H, L, and P) were captured through confocal microscopy at × 630 magnification ($n = 3$). Yellow arrow: AgNPs located inside the cytoplasm; blue, nucleus. Scale bar = 20 μm.

in vitro triple cell coculture BBB to reach neuronal cells and induce palmitic acid generation for Aβ accumulation in neuronal cells, leading to inflammatory cytokine secretion and apoptosis and potentially inducing AD progression.

AgNPs Disrupt Tight Junctions in bEnd.3 Cells

Tight junction proteins play a major role in protecting and maintaining brain homeostasis. This study observed that AgNPs disrupted tight junction proteins, ZO-1 and claudin-5, in bEnd.3 cells to enhance BBB permeability in the triple cell coculture model (Figure 2), and AgNPs were absorbed by ALT and N2a cells (Figure 3). Similar results were observed in *in vitro* double- and triple cell coculture models. Tang *et al.* (2010) revealed that AgNPs can cross the rat BBB to accumulate inside brain microvascular endothelial cells (BMVECs) and astrocytes in a double cell coculture model. Xu *et al.* (2015) showed that AgNPs reduce the gene expression of ZO-1, disrupt the tight junctions of brain endothelial cells, and induce nuclear atypia and mitochondrial shrinkage in astrocytes of a triple cell (BMCVECs, astrocytes, and pericytes) coculture model. Accordingly, AgNP exposure might enhance BBB permeability in inner neuronal cells by altering the protein expression of ZO-1 and claudin-5 to disrupt the tight junctions in brain endothelial cells.

AgNPs Modulated Fatty Acid Metabolism in Neuronal Cells

In this study, the concentration of AgNPs (1–4 μg/ml) converted to human exposure levels was 0.05–0.2 mg/kg/d. In a human study, the blood Ag concentration was 1.6 ± 0.4 mg/l after exposure to AgNPs (5–10 nm) at 10 μg/ml for 14 days (Munger *et al.*, 2014). Armitage *et al.* (1996) revealed that the Ag concentration in blood samples of workers with occupational Ag exposure ($n = 19$) and a control group ($n = 15$) was 1.3–20 and <0.1 μg/l, respectively. AgNPs influence the proteomic metabolism of LOVO human colon cancer cells (Verano-Braga *et al.*, 2014). In this study, Cytoscape gene-network analysis of DEPs indicated that AgNPs upregulate PPARα and PPARGC1α to activate CASP3 for apoptosis in N2a cells (Figure 4C). Furthermore, flow cytometric analysis revealed early and late apoptosis in N2a cells after AgNP exposure (Figure 6C). PPARα and PPARGC1α have been reported to regulate fatty acid metabolism through β-oxidation in C57BL/6J mouse liver mitochondria (Aharoni-Simon *et al.*, 2011; Poulsen *et al.*, 2012). Furthermore, PPARα activation has been reported to increase CASP3 activation and induce

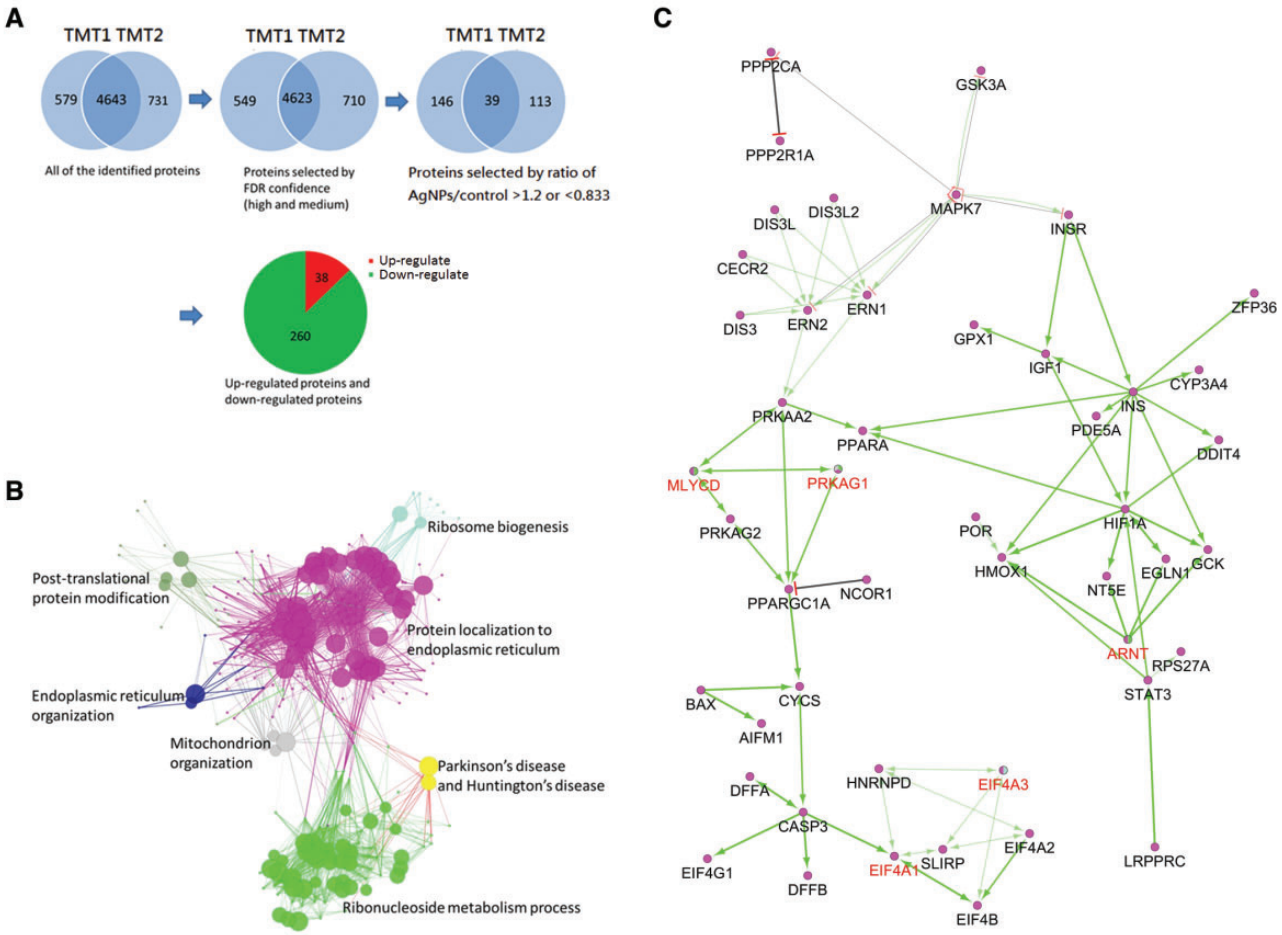

Figure 4. Proteomic and gene-network analysis in N2a cells after 4 μg/ml AgNP exposure. A, Venn diagrams of the total number of quantified proteins from two independent tandem mass tagging experiments (TMT1 and TMT2). A total of 5953 proteins were identified. After screening the total proteins based on FDR confidence (medium and high) and fold changes of TMT intensity (>1.2 or <0.833, ratio of AgNP exposure group to control group), 298 DEPs (upregulated, $n = 38$; downregulated, $n = 260$) were identified. B, A gene network was constructed using 298 DEPs. In the interaction networks, each node was represented as a cluster of genes, and the size and color of the nodes represented the fraction of the genes in the cluster with the same properties. C, Subnetwork of DEPs in N2a cells exposed to AgNPs. Green line, activation; blue line, binding; yellow line, expression; red line with a red bar, antagonizing.

Table 2. KEGG Pathway Analysis of DEPs After 4 μg/ml AgNPs Exposure

Term	Count	Genes	*P* Value
Ribosome	21	Fau, Mrp111, Mrp116, Mrps17, Mrps2, Rp113a, Rp121, Rp127, Rp128, Rp13, Rp130, Rp132, Rp135a, Rp17a, Rp19, Rps16, Rps23, Rps3, Rps7, Rps9, Rplp1	8.5E−13
Oxidative phosphorylation	11	Atp5q2, Atp6v0a1, Ndufa11, Ndufa4, Ndrfa8, Ndufs, Ndufv3, ND1, Cox7a1, Cox7b, Cox6c	1.9E−04
Huntington's disease	13	Atp5q2, Ndufa11, Ndufa4, Ndufa8, Ndufs5, Ndufv3, Tbpl1, Ap2m1, Cox7a1, Cox7b, Cox6c, Slc25a4, Slc25a5	2.2E−04
Parkinson's disease	14	Atp5q2, Ndufa11, Ndufa4, Ndufa8, Ndufs5, Ndufv3, ND1, Cox7a1, Cox7b, Cox6c, Prkaca, Prkacb, Slc25a4, Slc25a5,	2.4E−04
Glycosylphosphatidylinositol (GPI)-anchor biosynthesis	4	Gpaa1, Piqk, Piqn, Piqu	9.8E−03
Alzheimer's disease	9	Atp5q2, Ndufa11, Ndufa4, Ndufa8, Ndufs5, Ndufv3, Cox7a1, Cox7b, Cox6c	1.4E−02
Insulin signaling pathway	7	Araf, G6pc3, Makp9, Prkaq1, Prkaca, Prkacb, Tsc2	4.0E−02
N-glycan biosynthesis	4	Stt3a, Stt3b, Alq11, Rpn2	5.8E−02
Fatty acid elongation	3	Hacd3, Acot7, Hsd17b12	7.9E−02

hepatocyte apoptosis in mice (Richardson-Burns *et al.*, 2002; Xiao *et al.*, 2006). In addition, fatty acid determination in this study revealed that AgNP exposure increased the palmitic acid concentration in N2a cells (Table 3). Kwon *et al.* (2014) indicated that palmitic acid increases the phosphorylation of extracellular signal-regulated kinase 1/2, c-Jun aminoterminal kinase, and nuclear factor kappa B to induce inflammatory signaling in N2a cells. Palmitic acid can activate CASP3 and increase apoptosis in

Table 3. Fatty Acid Profile of Neuronal Cells After 4 μg/ml AgNPs Exposure

Number	RT (min)	Ratio of AgNPs/Control		Common Name	Lipid Name	Molecular Formula	Molecular Weight
		Peak Area					
		ALT Cells	N2a Cells				
1	30.04	1.02±0.03	1.35±0.03*	Palmitic acid	C16:0	$C_{16}H_{32}O_2$	370.330
2	34.11	1.01±0.02	0.81±0.02*	Octadecanoic acid	C18:0	$C_{18}H_{36}O_2$	398.358

Fatty acid profile of ALT cells and N2a cells were determined by GC-MSD.
*$P < .05$ compared with control group.

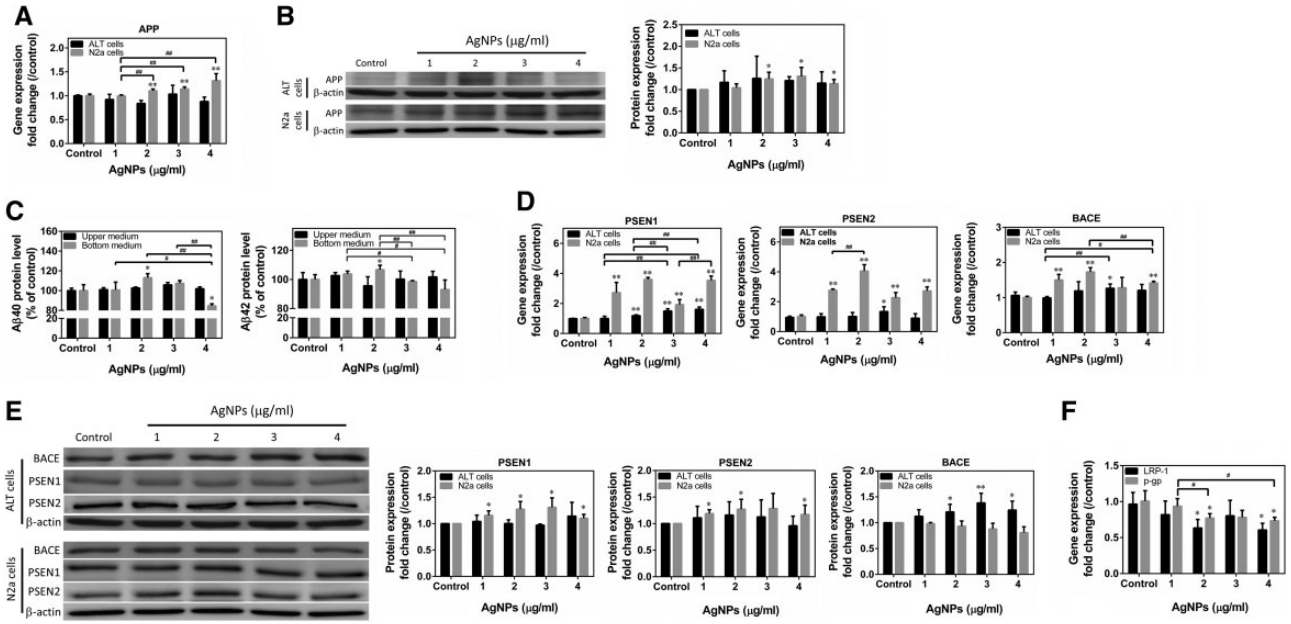

Figure 5. Detection of Aβ generation-related proteins and genes. After the triple cell coculture model was treated with AgNPs (1, 2, 3, and 4 μg/ml), the protein and gene expression of APP in ALT and N2a cells was determined through (A) real-time PCR ($n = 6$) and (B) Western blotting ($n = 4$), respectively. (C) The protein levels of Aβ40 and Aβ42 in the upper and bottom medium were evaluated using an ELISA kit. Results were represented in percentages compared with control group ($n = 4$). D, Gene expression and E, protein expression of Aβ generation-related secretases, namely PSEN1, PSEN2, and BACE, in ALT and N2a cells were examined through real-time PCR ($n = 6$) and Western blotting ($n = 4$), respectively, and F, gene expression of Aβ clearance-related receptors, LRP-1 and P-gp, in bEnd.3 cells was evaluated using real-time PCR ($n = 6$). Data were presented as the mean ± SD. These reactions were performed in duplicate in three independent experiments. *$P < .05$ and **$P < .01$, significantly different from the control group. #$P < .05$ and ##$P < .01$, significantly different between the two exposure groups.

neuron-like cells differentiated from PC12 rat adrenal medulla cells (Ulloth *et al.*, 2003). Hsiao *et al.* (2014) demonstrated that palmitic acid induces endoplasmic reticular stress and cell cycle arrest in the G2/M phase and accelerates Aβ accumulation and cell apoptosis through protein palmitoylation in SH-SY5Y human neuroblastoma cells. In C57BL/6 mice, palmitic acid increases reactive oxygen species levels, reduces neural progenitor cell concentration, disrupts hippocampal neurogenesis (Park *et al.*, 2011), increases membrane localization of protein kinase C-theta, and induces hypothalamic insulin resistance (Benoit *et al.*, 2009). These findings suggested that AgNP exposure might modulate fatty acid metabolism to increase the palmitic acid concentration and induce neuronal cell apoptosis.

AgNPs Induced Aβ Deposition and Inflammation for Neuronal Cell Apoptosis

Aβ accumulation in the brain is a pathological hallmark of AD progression. This study observed that AgNPs induced Aβ40 and Aβ42 secretion into the bottom medium with ALT and N2a cells (Figure 5C); however, Aβ40 and Aβ42 were not detected inside ALT and N2a cells (data not shown). Aβ40 and Aβ42 are common isoforms of Aβ, which is generated by β- and γ-secretase-mediated APP cleavage. Aβ40 and Aβ42 are typically produced in the trans-Golgi network and endoplasmic reticulum, respectively (Hartmann *et al.*, 1997), and can be secreted into the cerebrospinal fluid (CSF) of the brain (Maia *et al.*, 2015). In addition, the gene expression of Aβ clearance-related receptors, P-gp and LRP-1, was attenuated after AgNP exposure (Figure 5F), suggesting that AgNPs might impair Aβ clearance activity, resulting in Aβ accumulation in neuronal cells and subsequent cell apoptosis. P-gp is an ATP-binding cassette transporter that transports Aβ40/42 out of the brain endothelium (Lam *et al.*, 2001). In the brain of P-gp null mice, the Aβ clearance rate is reduced after Aβ40/42 injection into the CNS (Cirrito *et al.*, 2005). P-gp function is decreased significantly in patients with AD compared with non-AD patients (van Assema *et al.*, 2012). LRP-1 acts an important Aβ transporter from the brain to blood through brain endothelial cells (Wolf *et al.*, 2012). LRP-1-deficient mice exhibit reduced Aβ42 clearance activity through the BBB, increased brain Aβ42 levels, and impair learning ability and recognition

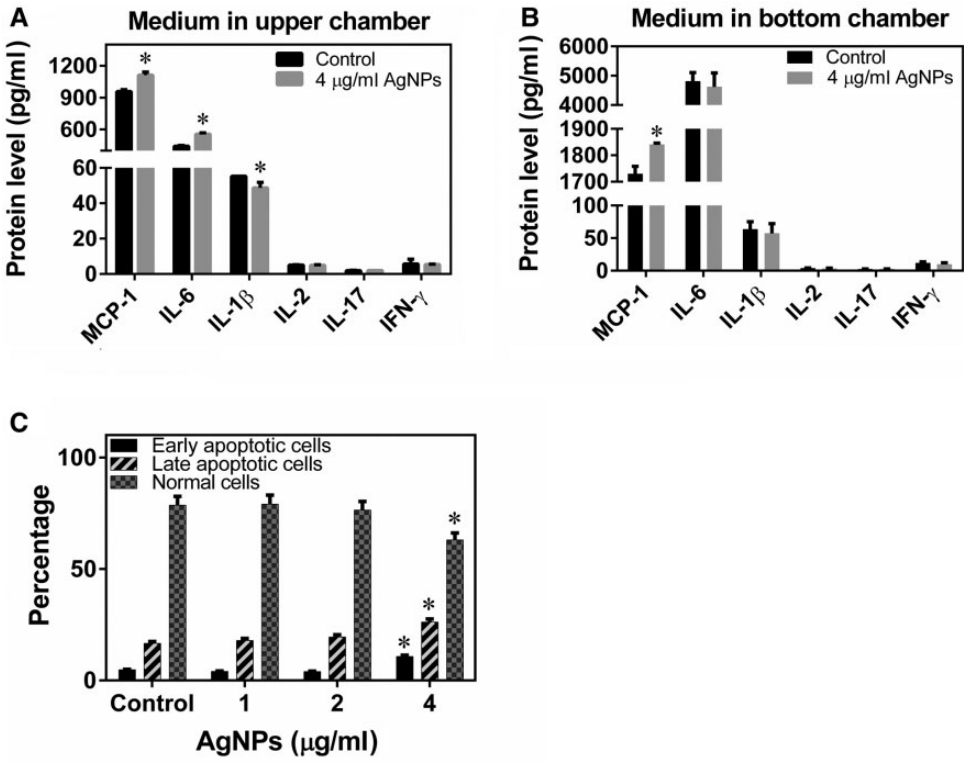

Figure 6. Inflammatory cytokine secretion and cell apoptosis in the triple cell coculture model after AgNP exposure. After the triple cell coculture model was exposed to AgNPs at 4 μg/ml for 24 h, cytokine levels in the (A) upper medium and (B) bottom medium were determined using a cytokine assay kit ($n = 2$). Data were presented as the mean ± SD. C, Early and late apoptosis in N2a cells was detected using flow cytometry in the triple cell coculture model after AgNP exposure (1, 2, 3, and 4 μg/ml) for 24 h ($n = 3$). Results were presented as percentages of early apoptosis cells, late apoptosis cells, and normal cells. These assays were performed in duplicate in two independent experiments. *$P < .05$, significantly different from the control group.

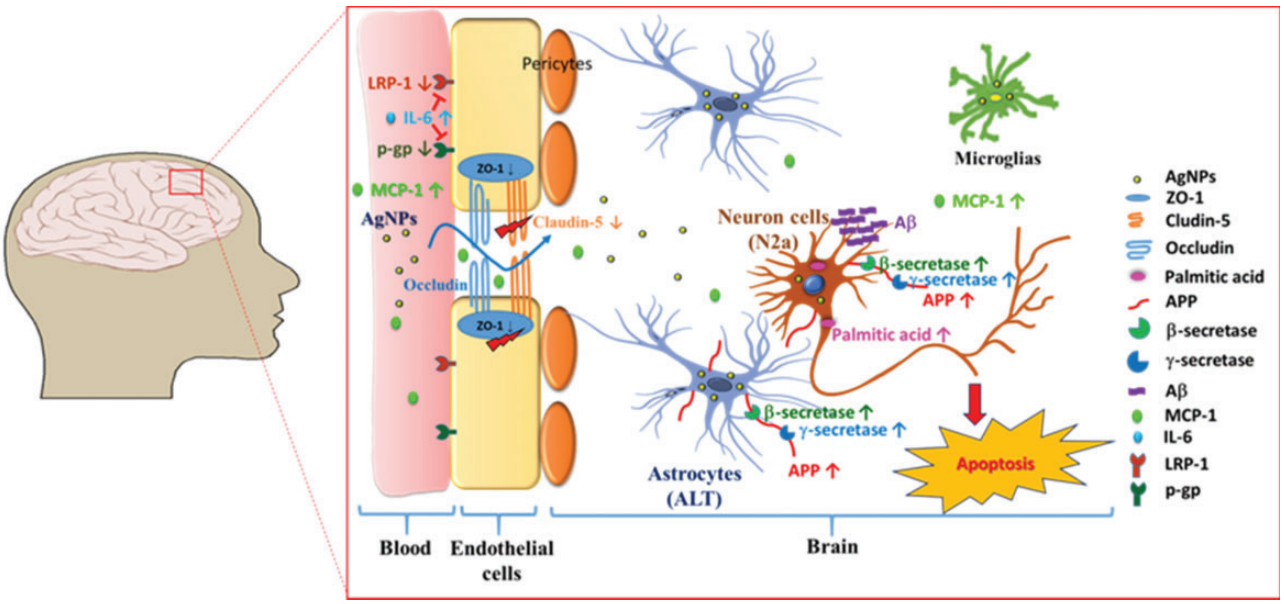

Figure 7. Schematic diagram of AgNP exposure in cerebral vascular endothelial cells, astrocytes, and neuronal cells inducing AD progression. AgNPs disrupt the tight junction proteins ZO-1 and claudin-5 in cerebral vascular endothelial cells to enhance BBB permeability. AgNPs can enter the brain and can be internalized by astrocytes and neuronal cells. AgNPs increase the palmitic acid concentration and enhance APP accumulation to promote Aβ generation in neuronal cells. Moreover, AgNPs induce the protein expression of Aβ generation-related secretases (PSEN1, PSEN2, and BACE) for digesting APP in astrocytes and neuronal cells into Aβ peptide fragments, which were subsequently released into the CSF. AgNPs also induce IL-6 secretion to attenuate the gene expression of Aβ clearance-related receptors (LRP-1 and P-gp) in brain endothelial cells, which impair Aβ clearance ability, resulting in Aβ accumulation in the CSF. These AgNP-induced Aβ proteins can further aggregate on the neuronal cell surface to stimulate an MCP-1-mediated inflammatory response, potentially leading to neuronal cell apoptosis and thus AD progression.

memory (Jaeger *et al.*, 2009). LRP-1 inhibitor-induced attenuation of LRP-1 protein activity increases Aβ40 accumulation in the brain of C57BL/6 mice (Shibata *et al.*, 2000). Furthermore, Aβ accumulation increases inflammatory responses in the brain of APP transgenic mice (Patel *et al.*, 2005), and Aβ-induced inflammation increases neuronal cell apoptosis (Palop and Mucke, 2010). In addition, this study revealed that AgNP exposure induces early and late apoptosis in N2a cells (Figure 6C).

This study also demonstrated that AgNPs enhanced MCP-1 and IL-6 secretion and attenuated IL-1β secretion into the upper medium with bEend.3 cells. In addition, AgNPs induced MCP-1 secretion into the bottom medium with ALT and N2a cells in the triple cell coculture model (Figs. 6A and B). Inflammation is a key factor in AD pathogenesis (Shadfar *et al.*, 2015). Miklossy and McGeer (2016) indicated that chronic bacterial infection induces inflammation and plays a crucial role in AD progression. IL-1β expression in human brain endothelial cells can prevent toxic mycobacteria from entering the brain (Corsini *et al.*, 1996). The present study revealed that AgNP exposure reduced IL-1β secretion in brain endothelial cells, which may reduce the activities for defense against bacterial infections in the brain and increase the risk of AD progression. MCP-1 has been demonstrated to recruit monocytes into the foci of active inflammation (Ajuebor *et al.*, 1998). MCP-1 secretion can be induced by Aβ40/42 in primary rat astrocytes (Johnstone *et al.*, 1999). Furthermore, increased MCP-1 levels might induce neuronal cell death (Katayama *et al.*, 2002). Sawyer *et al.* (2014) indicated that MCP-1 influences neuronal loss, which is integral to the progression of neurological disorders, such as AD and Parkinson disease, through BBB leakage and macrophage polarization. In addition, MCP-1 has been reported to induce the redistribution and disruption of ZO-1 and claudin-5 to increase BBB permeability in mouse monocultured brain endothelial cells (Stamatovic *et al.*, 2003) and a coculture model of mouse brain endothelial cells and astrocytes (Stamatovic *et al.*, 2005). IL-6 attenuates the expression of claudin-5 and occludin to enhance BBB permeability in the brain of adult sheep (Cohen *et al.*, 2013). Furthermore, IL-6 reduces LRP-1 expression in human microvascular endothelial cells (Kitazawa *et al.*, 2016) and attenuates P-gp activity in the cultured brain endothelial cells of fetal guinea pigs (Iqbal *et al.*, 2016). Moreover, increased MCP-1 and IL-6 levels have been observed in patients with mild AD (Cojocaru *et al.*, 2011; Galimberti *et al.*, 2006) and a rat AD model (El Dayem *et al.*, 2013; Patel *et al.*, 2005).

These findings indicate that AgNPs can disrupt tight junctions to reach neuronal cells, and AgNP-induced palmitic acid generation might increase Aβ secretion to induce an inflammatory response and attenuate Aβ clearance to stimulate neuronal cell apoptosis.

AgNP Exposure Potentially Induced AD Progression

Figure 7 depicted the potential pathway through which AgNPs induced AD progression according to the findings of this study. After entering the blood circulation system, AgNPs might disrupt the tight junction proteins of brain endothelial cells, ZO-1 and claudin-5, and enter through astrocytes to reach neuronal cells. These AgNPs may modulate fatty acid metabolism to increase palmitic acid generation, which could enhance Aβ accumulation, inflammation, and apoptosis in neuronal cells. In addition, Aβ is generated through β- and γ-secretase-mediated APP cleavage in neuronal cells, and is secreted into the CSF. AgNP exposure increased APP accumulation and induced the protein expression of Aβ generation-related secretases, PSEN1, PSEN2 (encoded for γ-secretases), and BACE (encoded for β-secretases), for APP cleavage in astrocytes and neuronal cells. Furthermore, AgNPs induced IL-6 secretion to attenuate the gene expression of Aβ clearance-related receptors, P-gp and LRP-1. Aβ can translocate from the CSF to the blood circulation system through the LRP-1 and P-gp of brain endothelial cells. Decreased LRP-1 and P-gp activity might promote Aβ accumulation in the CSF, and increased Aβ would aggregate on the neuronal cell surface to stimulate an MCP-1-mediated inflammatory response, leading to neuronal cell apoptosis and potentially inducing AD progression.

CONCLUSION

This study is the first to demonstrate that AgNP exposure disrupts tight junctions in a triple cell coculture model to promote palmitic acid generation, Aβ40 and Aβ42 deposition, and inflammatory cytokine secretion and to attenuate gene expression of Aβ clearance-related receptors, leading to neuronal cell apoptosis. AgNPs have been widely used in medical applications and consumer products; therefore, these findings highlighted the potential adverse effects of AgNP exposure, which may cause neurodegenerative disorders such as AD.

SUPPLEMENTARY DATA

Supplementary data are available at *Toxicological Sciences* online.

ACKNOWLEDGMENT

We thank Gold Nanotech, Inc., Taiwan for providing AgNPs material in this collaborative research.

FUNDING

This study was supported by Taiwan Ministry of Science and Technology grant 103-2221-E-007-006-MY3.

REFERENCES

Aharoni-Simon, M., Hann-Obercyger, M., Pen, S., Madar, Z., and Tirosh, O. (2011). Fatty liver is associated with impaired activity of PPAR gamma-coactivator 1 alpha (PGC1 alpha) and mitochondrial biogenesis in mice. *Lab. Invest.* **91**, 1018–1028.

Ajuebor, M. N., Flower, R. J., Hannon, R., Christie, M., Bowers, K., Verity, A., and Perretti, M. (1998). Endogenous monocyte chemoattractant protein-1 recruits monocytes in the zymosan peritonitis model. *J. Leukoc. Biol.* **63**, 108–116.

Armitage, S. A., White, M. A., and Wilson, H. K. (1996). The determination of silver in whole blood and its application to biological monitoring of occupationally exposed groups. *Ann. Occup. Hyg.* **40**, 331–338.

Basak, J. M., Verghese, P. B., Yoon, H., Kim, J., and Holtzman, D. M. (2012). Low-density lipoprotein receptor represents an apolipoprotein E-independent pathway of Abeta uptake and degradation by astrocytes. *J. Biol. Chem.* **287**, 13959–13971.

Bednarczyk, J., and Lukasiuk, K. (2011). Tight junctions in neurological diseases. *Acta Neurobiol. Exp. (Wars)* **71**, 393–408.

Benoit, S. C., Kemp, C. J., Elias, C. F., Abplanalp, W., Herman, J. P., Migrenne, S., Lefevre, A. L., Cruciani-Guglielmacci, C., Magnan, C., Yu, F., *et al.* (2009). Palmitic acid mediates hypothalamic insulin resistance by altering PKC-theta subcellular localization in rodents. *J. Clin. Invest.* **119**, 2577–2589.

Bloom, G. S. (2014). Amyloid-beta and tau: The trigger and bullet in Alzheimer disease pathogenesis. *JAMA Neurol.* **71**, 505–508.

Chen, I. C., Hsiao, I. L., Lin, H. C., Wu, C. H., Chuang, C. Y., and Huang, Y. J. (2016). Influence of silver and titanium dioxide nanoparticles on in vitro blood-brain barrier permeability. *Environ. Toxicol. Pharmacol.* **47**, 108–118.

Cirrito, J. R., Deane, R., Fagan, A. M., Spinner, M. L., Parsadanian, M., Finn, M. B., Jiang, H., Prior, J. L., Sagare, A., Bales, K. R., *et al.* (2005). P-glycoprotein deficiency at the blood-brain barrier increases amyloid-beta deposition in an Alzheimer disease mouse model. *J. Clin. Invest.* **115**, 3285–3290.

Citron, M., Westaway, D., Xia, W., Carlson, G., Diehl, T., Levesque, G., Johnson-Wood, K., Lee, M., Seubert, P., Davis, A., *et al.* (1997). Mutant presenilins of Alzheimer's disease increase production of 42-residue amyloid beta-protein in both transfected cells and transgenic mice. *Nat. Med.* **3**, 67–72.

Cohen, S. S., Min, M., Cummings, E. E., Chen, X., Sadowska, G. B., Sharma, S., and Stonestreet, B. S. (2013). Effects of interleukin-6 on the expression of tight junction proteins in isolated cerebral microvessels from yearling and adult sheep. *Neuroimmunomodulation* **20**, 264–273.

Cojocaru, I. M., Cojocaru, M., Miu, G., and Sapira, V. (2011). Study of interleukin-6 production in Alzheimer's disease. *Rom. J. Intern. Med.* **49**, 55–58.

Corsini, E., Dufour, A., Ciusani, E., Gelati, M., Frigerio, S., Gritti, A., Cajola, L., Mancardi, G. L., Massa, G., and Salmaggi, A. (1996). Human brain endothelial cells and astrocytes produce IL-1 beta but not IL-10. *Scand. J. Immunol.* **44**, 506–511.

Deane, R., Bell, R. D., Sagare, A., and Zlokovic, B. V. (2009). Clearance of amyloid-beta peptide across the blood-brain barrier: Implication for therapies in Alzheimer's disease. *CNS Neurol. Disord. Drug Targets* **8**, 16–30.

El Dayem, S. M., Ahmed, H. H., Metwally, F., Foda, F. M., Shalby, A. B., and Zaazaa, A. M. (2013). Alpha-chymotrypcin ameliorates neuroinflammation and apoptosis characterizing Alzheimer's disease-induced in ovarictomized rats. *Exp. Toxicol. Pathol.* **65**, 477–483.

Foldbjerg, R., Olesen, P., Hougaard, M., Dang, D. A., Hoffmann, H. J., and Autrup, H. (2009). PVP-coated silver nanoparticles and silver ions induce reactive oxygen species, apoptosis and necrosis in THP-1 monocytes. *Toxicol. Lett.* **190**, 156–162.

Galimberti, D., Fenoglio, C., Lovati, C., Venturelli, E., Guidi, I., Corra, B., Scalabrini, D., Clerici, F., Mariani, C., Bresolin, N., *et al.* (2006). Serum MCP-1 levels are increased in mild cognitive impairment and mild Alzheimer's disease. *Neurobiol. Aging* **27**, 1763–1768.

Hampel, H., and Shen, Y. (2009). Beta-site amyloid precursor protein cleaving enzyme 1 (BACE1) as a biological candidate marker of Alzheimer's disease. *Scand. J. Clin. Lab. Invest.* **69**, 8–12.

Hartmann, T., Bieger, S. C., Bruhl, B., Tienari, P. J., Ida, N., Allsop, D., Roberts, G. W., Masters, C. L., Dotti, C. G., Unsicker, K., *et al.* (1997). Distinct sites of intracellular production for Alzheimer's disease A beta40/42 amyloid peptides. *Nat. Med.* **3**, 1016–1020.

Hsiao, Y. H., Lin, C. I., Liao, H., Chen, Y. H., and Lin, S. H. (2014). Palmitic acid-induced neuron cell cycle G(2)/M arrest and endoplasmic reticular stress through protein palmitoylation in SH-SY5Y human neuroblastoma cells. *Int. J. Mol. Sci.* **15**, 20876–20899.

Huang, C. L., Hsiao, I. L., Lin, H. C., Wang, C. F., Huang, Y. J., and Chuang, C. Y. (2015). Silver nanoparticles affect on gene expression of inflammatory and neurodegenerative responses in mouse brain neural cells. *Environ. Res.* **136**, 253–263.

Iqbal, M., Baello, S., Javam, M., Audette, M. C., Gibb, W., and Matthews, S. G. (2016). Regulation of multidrug resistance P-glycoprotein in the developing blood-brain barrier: Interplay between glucocorticoids and cytokines. *J. Neuroendocrinol.* **28**, 12360.

Jaeger, L. B., Dohgu, S., Hwang, M. C., Farr, S. A., Murphy, M. P., Fleegal-DeMotta, M. A., Lynch, J. L., Robinson, S. M., Niehoff, M. L., Johnson, S. N., *et al.* (2009). Testing the neurovascular hypothesis of Alzheimer's disease: LRP-1 antisense reduces blood-brain barrier clearance, increases brain levels of amyloid-beta protein, and impairs cognition. *J. Alzheimers Dis.* **17**, 553–570.

Ji, J. H., Jung, J. H., Kim, S. S., Yoon, J. U., Park, J. D., Choi, B. S., Chung, Y. H., Kwon, I. H., Jeong, J., Han, B. S., *et al.* (2007). Twenty-eight-day inhalation toxicity study of silver nanoparticles in Sprague-Dawley rats. *Inhal. Toxicol.* **19**, 857–871.

Johnstone, M., Gearing, A. J., and Miller, K. M. (1999). A central role for astrocytes in the inflammatory response to beta-amyloid; chemokines, cytokines and reactive oxygen species are produced. *J. Neuroimmunol.* **93**, 182–193.

Katayama, T., Minami, M., Nakamura, M., Ito, M., Katsuki, H., Akaike, A., and Satoh, M. (2002). Excitotoxic injury induces production of monocyte chemoattractant protein-1 in rat cortico-striatal slice cultures. *Neurosci. Lett.* **328**, 277–280.

Kitazawa, M., Hsu, H. W., and Medeiros, R. (2016). Copper exposure perturbs brain inflammatory responses and impairs clearance of amyloid-beta. *Toxicol. Sci.* **152**, 194–204.

Kwon, B., Lee, H. K., and Querfurth, H. W. (2014). Oleate prevents palmitate-induced mitochondrial dysfunction, insulin resistance and inflammatory signaling in neuronal cells. *Biochim. Biophys. Acta* **1843**, 1402–1413.

Lam, F. C., Liu, R., Lu, P., Shapiro, A. B., Renoir, J. M., Sharom, F. J., and Reiner, P. B. (2001). Beta-amyloid efflux mediated by p-glycoprotein. *J. Neurochem.* **76**, 1121–1128.

Leon, I. R., Schwammle, V., Jensen, O. N., and Sprenger, R. R. (2013). Quantitative assessment of in-solution digestion efficiency identifies optimal protocols for unbiased protein analysis. *Mol. Cell Proteomics* **12**, 2992–3005.

Li, G., Simon, M. J., Cancel, L. M., Shi, Z. D., Ji, X., Tarbell, J. M., Morrison, B., 3rd., and Fu, B. M. (2010). Permeability of endothelial and astrocyte cocultures: *In vitro* blood-brain barrier models for drug delivery studies. *Ann. Biomed. Eng.* **38**, 2499–2511.

Lin, H. C., Huang, C. L., Huang, Y. J., Hsiao, I. L., Yang, C. W., and Chuang, C. Y. (2016). Transcriptomic gene-network analysis of exposure to silver nanoparticle reveals potentially neurodegenerative progression in mouse brain neural cells. *Toxicol. in Vitro* **34**, 289–299.

Liu, W. Y., Wang, Z. B., Zhang, L. C., Wei, X., and Li, L. (2012). Tight junction in blood-brain barrier: An overview of structure, regulation, and regulator substances. *CNS Neurosci. Ther.* **18**, 609–615.

Maia, L. F., Kaeser, S. A., Reichwald, J., Lambert, M., Obermueller, U., Schelle, J., Odenthal, J., Martus, P., Staufenbiel, M., and Jucker, M. (2015). Increased CSF A during the very early phase of cerebral A deposition in mouse models. *EMBO Mol. Med.* **7**, 895–903.

Masuda, T., Tomita, M., and Ishihama, Y. (2008). Phase transfer surfactant-aided trypsin digestion for membrane proteome analysis. *J. Proteome Res.* **7**, 731–740.

Miklossy, J., and McGeer, P. L. (2016). Common mechanisms involved in Alzheimer's disease and type 2 diabetes: A key role of chronic bacterial infection and inflammation. *Aging (Albany, NY)* **8**, 575–588.

Munger, M. A., Radwanski, P., Hadlock, G. C., Stoddard, G., Shaaban, A., Falconer, J., Grainger, D. W., and Deering-Rice, C. E. (2014). In vivo human time-exposure study of orally dosed commercial silver nanoparticles. *Nanomedicine* **10**, 1–9.

Musch, M. W., Walsh-Reitz, M. M., and Chang, E. B. (2006). Roles of ZO-1, occludin, and actin in oxidant-induced barrier disruption. *Am. J. Physiol. Gastrointest. Liver Physiol.* **290**, G222–G231.

Oberdorster, G., Sharp, Z., Atudorei, V., Elder, A., Gelein, R., Kreyling, W., and Cox, C. (2004). Translocation of inhaled ultrafine particles to the brain. *Inhal. Toxicol.* **16**, 437–445.

Palop, J. J., and Mucke, L. (2010). Amyloid-beta-induced neuronal dysfunction in Alzheimer's disease: From synapses toward neural networks. *Nat. Neurosci.* **13**, 812–818.

Park, H. R., Kim, J. Y., Park, K. Y., and Lee, J. (2011). Lipotoxicity of palmitic acid on neural progenitor cells and hippocampal neurogenesis. *Toxicol. Res.* **27**, 103–110.

Patel, N. S., Paris, D., Mathura, V., Quadros, A. N., Crawford, F. C., and Mullan, M. J. (2005). Inflammatory cytokine levels correlate with amyloid load in transgenic mouse models of Alzheimer's disease. *J. Neuroinflammation* **2**, 9.

Poulsen, L., Siersbaek, M., and Mandrup, S. (2012). PPARs: Fatty acid sensors controlling metabolism. *Semin. Cell Dev. Biol.* **23**, 631–639.

Richardson-Burns, S. M., Kominsky, D. J., and Tyler, K. L. (2002). Reovirus-induced neuronal apoptosis is mediated by caspase 3 and is associated with the activation of death receptors. *J. Neurovirol.* **8**, 365–380.

Sawyer, A. J., Tian, W., Saucier-Sawyer, J. K., Rizk, P. J., Saltzman, W. M., Bellamkonda, R. V., and Kyriakides, T. R. (2014). The effect of inflammatory cell-derived MCP-1 loss on neuronal survival during chronic neuroinflammation. *Biomaterials* **35**, 6698–6706.

Shadfar, S., Hwang, C. J., Lim, M. S., Choi, D. Y., and Hong, J. T. (2015). Involvement of inflammation in Alzheimer's disease pathogenesis and therapeutic potential of anti-inflammatory agents. *Arch. Pharm. Res.* **38**, 2106–2119.

Shibata, M., Yamada, S., Kumar, S. R., Calero, M., Bading, J., Frangione, B., Holtzman, D. M., Miller, C. A., Strickland, D. K., Ghiso, J., *et al.* (2000). Clearance of Alzheimer's amyloid-ss(1-40) peptide from brain by LDL receptor-related protein-1 at the blood-brain barrier. *J. Clin. Invest.* **106**, 1489–1499.

Sinha, S., and Lieberburg, I. (1999). Cellular mechanisms of beta-amyloid production and secretion. *Proc. Natl. Acad. Sci. U.S.A.* **96**, 11049–11053.

Smolarkiewicz, M., Skrzypczak, T., and Wojtaszek, P. (2013). The very many faces of presenilins and the gamma-secretase complex. *Protoplasma* **250**, 997–1011.

Speranza, A., Crinelli, R., Scoccianti, V., Taddei, A. R., Iacobucci, M., Bhattacharya, P., and Ke, P. C. (2013). In vitro toxicity of silver nanoparticles to kiwifruit pollen exhibits peculiar traits beyond the cause of silver ion release. *Environ. Pollut.* **179**, 258–267.

Stamatovic, S. M., Keep, R. F., Kunkel, S. L., and Andjelkovic, A. V. (2003). Potential role of MCP-1 in endothelial cell tight junction 'opening': Signaling via Rho and Rho kinase. *J. Cell Sci.* **116**, 4615–4628.

Stamatovic, S. M., Shakui, P., Keep, R. F., Moore, B. B., Kunkel, S. L., Van Rooijen, N., and Andjelkovic, A. V. (2005). Monocyte chemoattractant protein-1 regulation of blood-brain barrier permeability. *J. Cereb. Blood Flow Metab.* **25**, 593–606.

Tan, K. P., Ho, M. Y., Cho, H. C., Yu, J., Hung, J. T., and Yu, A. L. (2016). Fucosylation of LAMP-1 and LAMP-2 by FUT1 correlates with lysosomal positioning and autophagic flux of breast cancer cells. *Cell Death Dis.* **7**, e2347.

Tang, J., Xiong, L., Wang, S., Wang, J., Liu, L., Li, J., Yuan, F., and Xi, T. (2009). Distribution, translocation and accumulation of silver nanoparticles in rats. *J. Nanosci. Nanotechnol.* **9**, 4924–4932.

Tang, J. L., Xiong, L., Zhou, G. F., Wang, S., Wang, J. Y., Liu, L., Li, J. G., Yuan, F. Q., Lu, S. F., Wan, Z. Y., *et al.* (2010). Silver nanoparticles crossing through and distribution in the blood-brain barrier in vitro. *J. Nanosci. Nanotechnol.* **10**, 6313–6317.

Trickler, W. J., Lantz, S. M., Murdock, R. C., Schrand, A. M., Robinson, B. L., Newport, G. D., Schlager, J. J., Oldenburg, S. J., Paule, M. G., Slikker, W., Jr, *et al.* (2010). Silver nanoparticle induced blood-brain barrier inflammation and increased permeability in primary rat brain microvessel endothelial cells. *Toxicol. Sci.* **118**, 160–170.

Ulloth, J. E., Casiano, C. A., and De Leon, M. (2003). Palmitic and stearic fatty acids induce caspase-dependent and -independent cell death in nerve growth factor differentiated PC12 cells. *J. Neurochem.* **84**, 655–668.

van Assema, D. M., Lubberink, M., Bauer, M., van der Flier, W. M., Schuit, R. C., Windhorst, A. D., Comans, E. F., Hoetjes, N. J., Tolboom, N., Langer, O., *et al.* (2012). Blood-brain barrier P-glycoprotein function in Alzheimer's disease. *Brain* **135**, 181–189.

Verano-Braga, T., Miethling-Graff, R., Wojdyla, K., Rogowska-Wrzesinska, A., Brewer, J. R., Erdmann, H., and Kjeldsen, F. (2014). Insights into the cellular response triggered by silver nanoparticles using quantitative proteomics. *ACS Nano* **8**, 2161–2175.

Wisniewski, J. R., Zougman, A., Nagaraj, N., and Mann, M. (2009). Universal sample preparation method for proteome analysis. *Nat. Methods* **6**, 359–362.

Wolf, A., Bauer, B., and Hartz, A. M. (2012). ABC transporters and the Alzheimer's disease enigma. *Front. Psychiatry* **3**, 54.

Xiao, S., Anderson, S. P., Swanson, C., Bahnemann, R., Voss, K. A., Stauber, A. J., and Corton, J. C. (2006). Activation of peroxisome proliferator-activated receptor alpha enhances apoptosis in the mouse liver. *Toxicol. Sci.* **92**, 368–377.

Xu, F., Piett, C., Farkas, S., Qazzaz, M., and Syed, N. I. (2013). Silver nanoparticles (AgNPs) cause degeneration of cytoskeleton and disrupt synaptic machinery of cultured cortical neurons. *Mol. Brain* **6**, 29.

Xu, L., Dan, M., Shao, A., Cheng, X., Zhang, C., Yokel, R. A., Takemura, T., Hanagata, N., Niwa, M., and Watanabe, D. (2015). Silver nanoparticles induce tight junction disruption and astrocyte neurotoxicity in a rat blood-brain barrier primary triple coculture model. *Int. J. Nanomed.* **10**, 6105–6119.

Yamada, K., Hashimoto, T., Yabuki, C., Nagae, Y., Tachikawa, M., Strickland, D. K., Liu, Q., Bu, G., Basak, J. M., Holtzman, D. M., *et al.* (2008). The low density lipoprotein receptor-related protein 1 mediates uptake of amyloid beta peptides in an in vitro model of the blood-brain barrier cells. *J. Biol. Chem.* **283**, 34554–34562.

Yang, Y., and Rosenberg, G. A. (2011). Blood-brain barrier breakdown in acute and chronic cerebrovascular disease. *Stroke* **42**, 3323–3328.